Degradation of ciprofloxacin using UV-based advanced removal processes: comparison of persulfate-based advanced oxidation and sulfite-based advanced reduction processes

Hannah Milh [a], Xingyue Yu [a,b], Deirdre Cabooter [b], Raf Dewil [a,*]

[a] *KU Leuven, Department of Chemical Engineering, Process and Environmental Technology Lab, J. De Nayerlaan 5, B-2860 Sint-Katelijne-Waver, Belgium*

[b] *KU Leuven, Department of Pharmaceutical and Pharmacological Sciences, Pharmaceutical Analysis, Herestraat 49, 3000 Leuven, Belgium*

**e-mail: raf.dewil@kuleuven.be (R. Dewil)*

Abstract

In this study, the degradation of ciprofloxacin (CIP) in wastewater was investigated using UV-based sulfate radical advanced oxidation processes (SR-AOP) and UV-based advanced reduction processes (ARP). More specifically, a comparison of the UV-based persulfate advanced oxidation process (the UV/PS process) and the UV-based sulfite advanced reduction process (the UV/sulfite process) was made. As for the UV-based SR-AOPs, the UV/PS process was much more efficient than the UV-based peroxymonosulfate advanced oxidation process (the UV/PMS process), with pseudo first order reaction rate constants (k_{obs}) of 0.752 and 0.145 min^{-1}, respectively. For the UV-based ARPs, the UV/sulfite process was the most efficient, compared to the UV/sulfide and the UV/dithionite process (k_{obs} of 0.269, 0.0157 and 0.0329 min^{-1}, respectively). The optimal process parameters for both the UV/PS and the UV/sulfite process were determined and the contribution of the produced reactive species were identified. For the UV/PS process, maximal CIP degradation was found at pH 8, and both •OH and $•SO_4^-$ were responsible for CIP degradation. For the UV/sulfite process, •H and $•e_{aq}^-$ were responsible for CIP degradation, with $•e_{aq}^-$ being the predominant radical at pH 8.5. Although CIP degradation was much faster for the UV/PS process, the UV/sulfite process was determined to be much more efficient in the defluorination of CIP.

Keywords

Sulfate radical based advanced oxidation processes – advanced reduction processes – ciprofloxacin – defluorination

1. Introduction

The presence of contaminants of emerging concern (CECs) in the aquatic environment is a widely known problem nowadays. CECs (pharmaceuticals, personal care products, endocrine-disrupting compounds,..) are increasingly found in the aquatic environment mainly due to their inefficient removal by conventional wastewater treatment processes (Kim et al., 2018; Petrie et al., 2014; Taheran et al., 2018). These CECs pose a serious threat to the aquatic environment due to their possible chronic toxicity on aquatic organisms, even if they are present at very low concentrations. A thorough and in-depth knowledge is currently lacking to assess the real risk that comes along with the presence of these substances on a long-term basis. Moreover, these emerging compounds are not individually present in the aquatic environment, but are found in mixtures. The literature has stated that mixtures of certain compounds may exhibit synergistic effects, enlarging the already existing problem of possibly chronic toxicity (Mezzelani et al., 2018; Petrie et al., 2014). Additionally, there is a limited understanding of the fate of these compounds once they enter the environment: it is not clear whether they are preferentially present in the soil or the aquatic phase (Petrie et al., 2014). Because of this lack of knowledge, various countries are currently working on the development of a legal framework regarding the presence of CECs (Caliman and Gavrilescu, 2009; Ebele et al., 2017; Mezzelani et al., 2018; Taheran et al., 2018). In Europe, this development is supported by severely increasing efforts to monitor CECs in natural water bodies, as stated in the EU Water Framework Directive (2000/60/EC), where a list of priority substances was proposed and is frequently updated. However, in developing countries, this is much less the case, complicating this challenge (Fekadu et al., 2019).

Besides the above mentioned problems, pharmaceuticals and more specifically antibiotics, pose an even bigger threat because of their role in the development of antibiotic resistant genes

(Gadipelly et al., 2014; Taheran et al., 2018). Hence, the removal of these compounds from wastewater is a priority.

Conventional wastewater treatment processes are insufficient for the removal of most emerging compounds (Petrie et al., 2014). Therefore, various advanced removal processes have been proposed, such as the use of ozone (O_3), hydrogen peroxide (H_2O_2), a combination of O_3 and H_2O_2 (peroxone process), Fenton and Fenton-like processes, … (Boczkaj and Fernandes, 2017; Dewil et al., 2017). In this study, two distinct but complementary processes regarding their performance in the removal of organic contaminants are investigated: sulfate radical based advanced oxidation processes (SR-AOPs) and advanced reduction processes (ARPs) using sulfur-based precursors. The main similarity uniting both processes is their mechanism of action: both processes rely on the production of reactive species which efficiently react with the target contaminant (Wacławek et al., 2017; Xiao et al., 2017b). The main difference between both processes is the nature of the produced reactive species: SR-AOPs produce highly oxidizing reactive species (e.g., $\bullet SO_4^-$ (mainly) and •OH), whereas ARPs rely on the production of highly reducing species ($\bullet SO_3^-$, $\bullet e_{aq}^-$,•H, $\bullet SO_2^-$ and HS^{*-}) (Wacławek et al., 2017; Yu et al., 2018), leading to a degradation of the target contaminant via an oxidative or reductive pathway, respectively. Furthermore, ARPs are specifically suitable for the treatment of halogenated organics (which are less prone to oxidation), efficiently breaking the carbon-halogen bond by introducing reactive reducing species (Li et al., 2012; Yang et al., 2020). SR-AOPs in general, however, are found to be suitable to degrade a myriad of molecules, because they combine the selective nature of $\bullet SO_4^-$ (reaction mainly through electron transfer) and the non-selective nature of •OH (various reaction routes with equal preference) (Ghanbari and Moradi, 2017). A disadvantage of SR-AOP is that the formed degradation products can exhibit a higher toxicity than the original target compound, while for ARP, the toxicity of the formed degradation products is generally lower (García-Galán et al., 2016; Yu et al., 2013).

Both SR-AOP and ARP rely on the activation of specific precursors to produce their respective reactive species. In order to conduct a reasonable comparison between ARP and AOP processes, UV-based activation processes are investigated in this study.

In SR-AOPs, oxidizing radicals are produced under UV irradiation using two different precursors/oxidants: (*i*) peroxydisulfate (PS, $S_2O_8^{2-}$) and (*ii*) peroxymonosulfate (PMS, HSO_5^-). The radicals are produced according to Eqs. (1) and (2) for PS and PMS, respectively. With an oxidation potential of 2.5-3.1 V for $\bullet SO_4^-$ and 2.8 V for •OH, these reactive species are considered to be highly oxidizing (Wang and Wang, 2018; Xie et al., 2015). Other activation methods of these precursors include activation using heat, transition metals, ultrasound, … (Fedorov et al., 2020; Wang and Wang, 2018).

UV/PS: $$S_2O_8^{2-} \xrightarrow{UV} 2 \bullet SO_4^- \quad (1)$$

UV/PMS: $$HSO_5^- \xrightarrow{UV} \bullet SO_4^- + \bullet OH \quad (2)$$

For ARP processes, reducing radicals can be produced using three types of precursors/reductants: (*i*) sulfite (SO_3^{2-}), (*ii*) dithionite ($S_2O_4^{2-}$) and (*iii*) sulfide (S^{2-}). Here, the reactive species are produced according to Eqs. (3)-(4), (5) and (6), respectively. It has been reported that $\bullet e_{aq}^-$ and •H have a reduction potential of 2.9 V and 2.7 V, respectively (Xiao et al., 2017a). $\bullet SO_3^-$, however, has an estimated reduction potential of 0.63 V only, and contributes mainly to the transformation between radicals, while $\bullet SO_2^-$ and HS^{*-} have a reduction potential of 0.66 V and 0.45 V, respectively (Mayhew, 1978; Melsheimer and Schlögl, 1997; Neta and Huie, 1985).

UV/sulfite: $$SO_3^{2-} \xrightarrow{UV} \bullet SO_3^- + \bullet e_{aq}^- \quad \text{(pH>7)} \quad (3)$$

$$HSO_3^- \xrightarrow{UV} \bullet SO_3^- + \bullet H \quad \text{(pH<7)} \quad (4)$$

UV/dithionite: $S_2O_4^{2-} \xrightarrow{UV} 2 \bullet SO_2^-$ (5)

UV/sulfide: $HS^- \xrightarrow{UV} HS^{*-}_{\text{(excited state)}}$ (6)

In this study, the above discussed processes are tested for the degradation of ciprofloxacin (CIP), an antibiotic fluoroquinolone compound, which is used to treat several bacterial infections. Among the antibiotic compounds, fluoroquinolone compounds are most frequently detected in the aquatic environment. A study by Johnson *et al*. (2015) stated that the consumption of ciprofloxacin in Europe was estimated to be 0.652 mg/cap/day, compared to 0.418 mg/cap/day and 0.82 mg/cap/day for the commonly used antibiotics trimethoprim and sulfamethoxazole, respectively (Guo et al., 2017; Johnson et al., 2015).

The aim of this research is to investigate the potential of different UV-based SR-AOP/ARP processes for the degradation of CIP and to select the best performing SR-AOP and ARP processes. Hereafter, the influence of different process parameters for the best SR-AOP and ARP processes is investigated and compared. Additionally, the release of fluorine from CIP is an interesting parameter to compare the degradation mechanism of the optimized SR-AOP and ARP processes, and confirm the benefits of ARP as a dehalogenation process.

2. Materials and methods

2.1 Chemicals

High purity CIP was purchased from Sigma-Aldrich. A stock solution of CIP (120.84 µM) was prepared in Milli-Q water, and diluted 2 times in ultrapure water for the degradation experiments, resulting in a concentration of 60.42 µM. Sodium sulfite (Na_2SO_3) and sodium dithionite ($Na_2S_2O_4$) were purchased from Fisher Chemical (≥ 97%), and sodium sulfide (Na_2S) was purchased from Acros Organics. HPLC grade acetonitrile (ACN) and formic acid (FA) were obtained from Fisher Chemical (≥ 97%) and Honeywell (≥98%), while ammonium

formate (99%) was obtained from Acros Organics. For the Ion Chromatography (IC) analysis, sodium bicarbonate ($NaHCO_3$, Fisher Chemical, 99.5+%), sodium carbonate (Na_2CO_3, Merck), nitric acid (HNO_3, Acros Organics, 65%), 2,6-pyridinedicarboxylic acid (DPA, Sigma Aldrich, 99%) and oxalic acid (Acros organics, 98%) were used. Methanol (MeOH, Acros Organics, HPLC grade), sodium hydroxide (NaOH, Acros Organics), sulfuric acid (H_2SO_4, Fisher Chemical, >95%), ethanol (EtOH, Fisher Chemical, analytical reagent grade), t-butanol (TBA, Acros Organics, 99.5%), potassium iodide (KI, Acros Organics, 99+%), sodium bicarbonate ($NaHCO_3$, VWR, reagent grade), peroxymonosulfate (PMS, HSO_5^-) in the form of oxone ($KHSO_5.0.5KHSO_4.0.5K_2SO_4$, Merck, synthesis grade) and potassium persulfate ($K_2S_2O_8$, Fisher Scientific, reagent grade) were used in the experiments. All solutions were prepared with Milli-Q water purified using a Milli-Q Millipore system (18MΩ cm^{-1}) (Merck).

2.2 Experimental set-up

All experiments were conducted in a sealed lab-scale cylindrical photo-reactor, similar as in previous research (Yu et al., 2020). A quartz tube was located centrally in the reactor containing a low-pressure UV mercury lamp (Phillips TUV PL-L, Poland, with a wavelength of approximately 253.4 nm). The light source was switched on for at least 5 min prior to starting the experiments to pre-heat and obtain a stable photo flux output. For the ARP experiments, the reaction mixture was purged with nitrogen gas to displace any dissolved oxygen in the system before starting any experiment. A homogeneous reaction mixture was obtained by continuous stirring. The temperature of the reaction mixture can be significantly influenced by the heat emitted by the UV lamp during the irradiation process. Therefore, the reaction mixture was constantly cooled by circulating tap water around the reactor.

For the degradation experiments, a predefined stock solution of CIP and the oxidant/reductant were mixed (total volume of 800 mL and an initial CIP concentration of 60.42μM) and subsequently exposed to UV irradiation. During the reaction, approximately 2 mL of sample

was taken from the reaction mixture at regular time intervals and transferred to vials for further analysis. For the SR-AOP experiments, methanol was added to the samples to avoid degradation of CIP by residual oxidant present in the sample. Therefore, 0.5 mL of methanol was added to a vial containing 0.5 mL of sample. For the ARP experiments, the reduction of CIP in a reaction mixture with sulfite only was observed to be negligible (less than 1% degradation in 48 h at a sulfite dosage of 1 mM), so the residual CIP concentration was analyzed within 12 h without quenching the residual sulfite in the sample. In first instance, the combination of UV with different reagents (oxidants and reductants) was tested to compare their abilities in degrading CIP and to screen the most promising oxidant/reductant for further study. Hereafter, one type of oxidant/reductant was chosen and used for further experiments. The influence of the oxidant/reductant dosage, UV power (5, 9 and 18 W) and initial pH value were studied in batch experiments. To evaluate the contributions of various radicals produced in the reaction mixture during the CIP degradation, radical scavenging experiments (for both the ARP and AOP processes) were conducted at different initial pH. The fluoride (F^-) concentration was analyzed to explore the difference in defluorination efficiency for both processes. All experiments were performed at least in duplicate to observe the reproducibility and average values are reported.

2.3 Analytical techniques

The CIP concentration was analyzed using High Performance Liquid Chromatography (HPLC-UV). An Agilent 1100 HPLC system (Agilent Technologies, Waldbronn, Germany) was used. The system consisted of a quaternary pump, an autosampler and a VWD detector (280 nm). The separation was carried out using a C18 column (Zorbax Eclipse Plus, 4.6 x 100 mm; particle size (d_p): 3.5 μm). As mobile phases, (A) 10 mM ammonium formate in water, adjusted to pH 2.8 with FA and (B) ACN were used. The analysis method consisted of a gradient, starting from 10% B and linearly increasing to 15% B in 15 min. Hereafter, the column was reconditioned

for 5 min at the initial conditions. The flow rate was set at 1 mL/min and the injection volume was 3 µL. The CIP calibration curve was constructed at 8 concentration levels (1-50 ppm). A linear calibration curve regression with a coefficient of determination (R^2) > 0.999 was obtained. The limit of detection (LOD, S/N ≥ 3, n=5) and quantification (LOQ, S/N ≥ 10, n=5) were determined to be xxx and xxx, respectively.

The residual PS concentration was measured similar as in previous research (Milh et al., 2020). Fluoride concentrations in the samples were measured using Ion Chromatography (IC). A 883 Basic IC Plus system (Metrohm) was used, equipped with a Metrosep A Supp 5 anion column (Metrohm, 250 x 4.0mm, d_p: 5µm) and a Metrosep C6 cation column (Metrohm, 150 x 4.0mm, d_p: 5µm). As mobile phases, 1 mM $NaHCO_3$ and 3.2 mM Na_2CO_3 in water were used for the anion eluent and 1.7 mM HNO_3 and 1.7 mM DPA in water was used for the cation eluent. The suppressor acid consisted of 500 mM H_2SO_4 and 100 mM oxalic acid in water. The injection volume was 20 µL. All solutions were made in ultrapure water and degassed prior use. The calibration curve for fluoride ions was constructed at 5 concentration levels (0.1-2.5 ppm). A linear calibration curve regression with a coefficient of determination (R^2) > 0.999 was obtained. The limit of detection (LOD, S/N ≥ 3, n=5) and quantification (LOQ, S/N ≥ 10, n=5) were determined to be xxx and xxx, respectively.

3. Results and discussion

3.1 Screening: ARP vs. AOP

First, different AOP and ARP processes were tested for the removal of CIP. The best SR-AOP process was then further compared with the best ARP process.

For the SR-AOP processes, the UV/PS and the UV/PMS process were evaluated. The results are shown in Fig. 1. Both processes were found to fit a pseudo first order kinetic model well.

Similar to Sharma *et al.* (2015), the pseudo first order reaction kinetics model was fit to the obtained degradation profiles (for both AOP and ARP processes). In this way, the observed reaction rate constants (k_{obs}) were determined for all experiments (Sharma et al., 2015). The pseudo first order fit is in agreement with several previous publications (Lin and Wu, 2014; Liu et al., 2013a, 2013b; Luo et al., 2016). The k_{obs} were 0.752 and 0.145 min^{-1} for the UV/PS and UV/PMS process at an oxidant dosage of 1.1 mM, respectively. The efficiency of the UV/PS process is hence much higher compared to the UV/PMS process, resulting in a full CIP degradation in only 10 min reaction time, compared to a CIP degradation of 79% after 10 min reaction time for the UV/PMS process. In these experiments, the pH of the solution was not adjusted, and was 6 and 3.3 for the UV/PS and the UV/PMS process, respectively (PMS is more acidic than PS). The obtained results are in agreement with the literature, where the UV/PS process was also found to be more efficient in degrading ciprofloxacin in distilled water than the UV/PMS process, even when both experiments were conducted at pH 7.5 (Mahdi-Ahmed and Chiron, 2014). Here, the decrease in degradation efficiency in the UV/PMS process was explained by the formation of the (less reactive) radical $\bullet SO_5^-$. Thus, the UV/PS process was chosen as the best AOP process for further comparison with ARP processes. The efficiency of this process also shows when calculating the synergistic coefficient (F), which resembles the enhancement in efficiency when combining UV with PS, compared to using only UV (results shown in paragraph 3.4) and PS, respectively. In a similar way to Ran and Li (2020), the synergistic coefficient was calculated for the UV/PS process and determined to be 10.7 (Ran and Li, 2020), indicating a significant enhancement of the CIP degradation when UV was combined with PS. The contribution of PS only to the degradation of CIP was found to be negligible over the observed reaction time.

For the ARP processes, the UV/sulfite, UV/dithionite and UV/sulfide processes were tested at the same reductant concentrations and pH conditions (pH 8.5). The results and conditions are

shown in Fig. 2. The highest degradation efficiency for CIP (99%) was obtained by the UV/sulfite process after 30 min reaction time. In contrast, the UV/dithionite and UV/sulfide processes led to much lower degradation efficiencies of around 32% and 55%, respectively. The obtained k_{obs} for the UV/sulfite process was 0.269 min^{-1}, while the k_{obs} for the UV/dithionite and the UV/sulfide process were 0.0157 and 0.0329 min^{-1}, respectively. Similar results were found in previous studies, where the difference in degradation efficiency was attributed to the different reductive capabilities of the reactive species generated in the different ARP processes (Liu et al., 2013a; Van Doorslaer et al., 2011). Consequently, the UV/sulfite process was regarded as the most effective for the degradation of CIP and will be further used in the following sections. The calculation of the synergistic coefficient for the UV/sulfite process, resulted in 2.5, which is much lower compared to 10.7 in the UV/PS process.

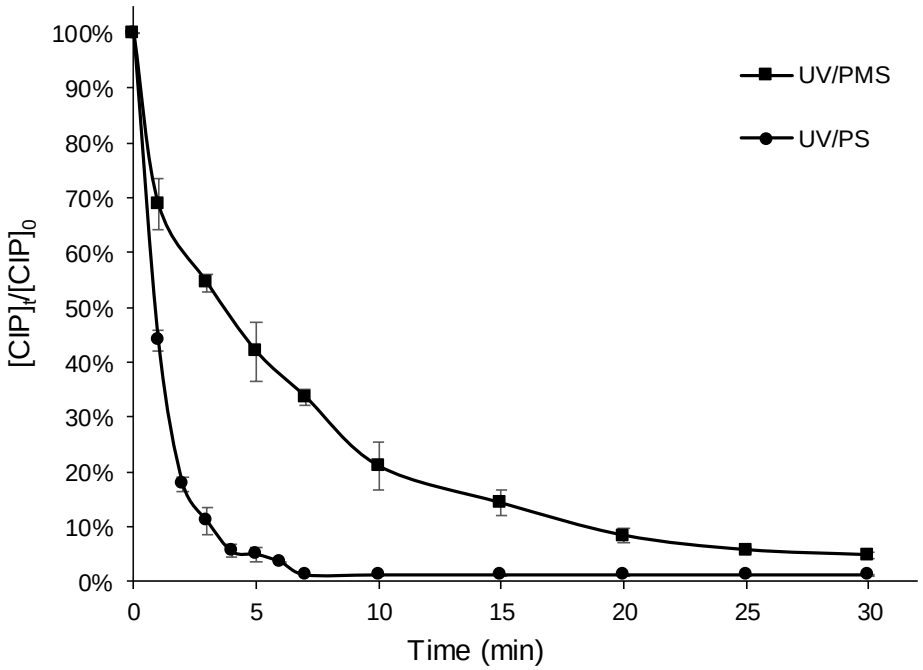

Fig. 1: Oxidant screening for CIP degradation: AOP system.
Conditions: $[CIP]_0$ = 60.42 µM, $[PS]_0 = [PMS]_0$ = 1.1 mM, UV power = 18 W.

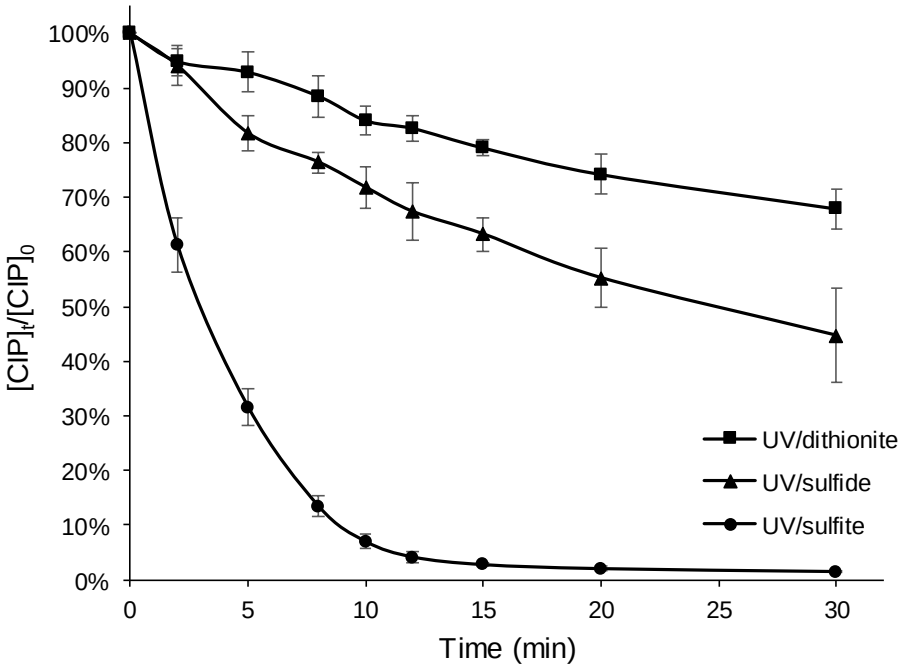

Fig. 2: Reductant screening for CIP degradation: ARP system.
Conditions: $[CIP]_0$ = 60.42 µM, $[Sulfite]_0$ = $[Dithionite]_0$ =$[Sulfide]_0$ = 1 mM, UV power = 18 W.

3.2 Influence of oxidant/reductant concentration

To investigate the influence of the oxidant/reductant dosage, different initial concentrations of PS/sulfite ($[PS]_0/[sulfite]_0$) were added to the reaction mixture. k_{obs} was determined for every experiment for both the SR-AOP and ARP processes. The results showed a similar trend for both SR-AOP and ARP processes (Fig. 3).

As shown in Fig. 3, for the UV/PS process, k_{obs} initially increases linearly with increasing $[PS]_0$ (at low $[PS]_0$, $k_{obs} = 1.028\times[PS]_0 + 0.0761$, $R^2 = 0.9507$). This linearity was also reported by Guo *et al.* (2017) (Guo et al., 2017). At higher $[PS]_0$, the increase in k_{obs} diminishes, indicating an inhibition of the degradation rate. These observations confirm results previously published by Khan *et al.* (2017), who investigated the UV/PMS process, and attributed the increase in k_{obs} at lower oxidant concentrations to an increase in radical formation. The inhibition at high oxidant concentration could be attributed to an increase in radical-radical and radical-persulfate

interactions (Khan et al., 2017). From these experiments, a $[PS]_0$ of 1.1 mM was chosen for further experiments.

For the UV/sulfite process, similar results were found: the k_{obs} values increased linearly (k_{obs} = $0.193 \times [sulfite]_0 + 0.0534$, $R^2 = 0.9225$) from 0.0703 to 0.269 min^{-1} as the sulfite dosage increased to 1 mM. When further increasing the sulfite concentration from 1 to 2 mM, k_{obs} only increased slightly from 0.269 to 0.297 min^{-1}. This trend can, in a similar way as the UV/PS process, be attributed to the occurrence of radical-radical interactions (Jung et al., 2015; Yazdanbakhsh et al., 2018).

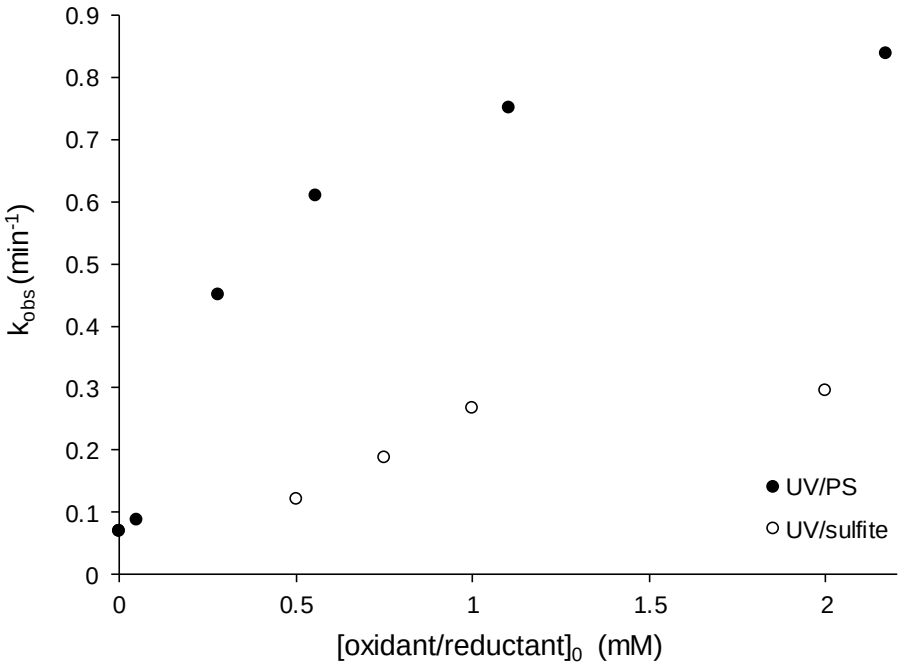

Fig. 3: k_{obs} as a function of initial oxidant/reductant concentration.
Conditions: $[CIP]_0$ = 60.42 µM, non-adjusted pH, UV power = 18 W.

3.3 Influence of UV intensity

Low-pressure UV lamps of different power (5, 9 and 18 W) were used to investigate the influence of the UV intensity on the degradation efficiency of CIP. For the UV/sulfite and the UV/PS process, the results are depicted in Fig. 4a and 4b, respectively. For the UV/PS process, a steep increase in k_{obs} can be observed with increasing UV power (an increase of a k_{obs} of

283 0.2051 min^{-1} at 5W to 0.752 min^{-1} at 18W). In the UV/sulfite process, the degradation rate
284 increased linearly from 0.084 to 0.269 min^{-1}.

285 This can be explained by the increase in number of photons released at higher power, leading
286 to a higher production of reactive species in both systems as well as an increase in direct UV
287 degradation of CIP (see further) (Kamel et al., 2009). Similar trends were found for the
288 UV/H_2O_2 process by Somathilake *et al*. (2019), by Kanjal *et al.* (2020), who investigated this
289 for the UV/PMS process and by Liu *et al.* (2013) who found this for the UV/sulfite process
290 (Kanjal et al., 2020; Liu et al., 2013b; Somathilake et al., 2019).

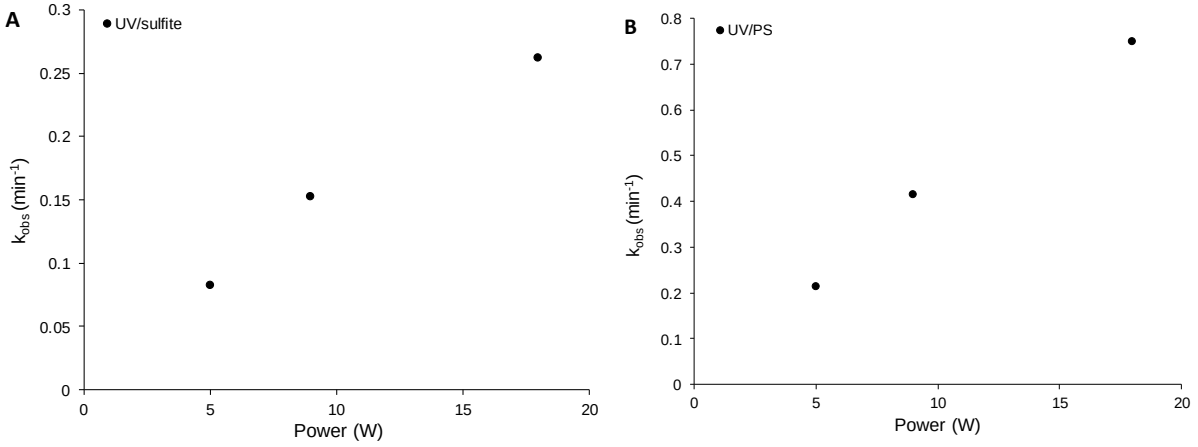

291

292 Fig. 4: k_{obs} as a function of UV lamp power for (A) the UV/sulfite and (B) the UV/PS process.
293 Conditions: $[CIP]_0$ = 60.42 µM, non-adjusted pH, (A) $[SO_3^{2-}]_0$ = 1 mM, (B) $[PS]_0$ = 1.1 mM.
294

295 **3.4 Influence of initial pH**

296 The SR-AOP and ARP degradation experiments were conducted at different initial pH values
297 to assess the influence of pH on the degradation efficiency. The pH of the solution has a
298 significant influence on (*i*) the ionization state of CIP, (*ii*) the ionization state of the
299 oxidant/reductant and (*iii*) the produced reactive species. It was chosen to conduct the
300 experiments at initial pH values of 3, 6, 8/8.5 (SR-AOP/ARP) and 10. Because no buffer was
301 used, the pH was free to change during the experiments. For every SR-AOP experiment, the

pH decreased to a final value of ± 3. For the ARP experiments, no significant pH change was observed during the selected reaction time.

The different ionization states of CIP over the range of relevant pH values are shown in Fig. 5.

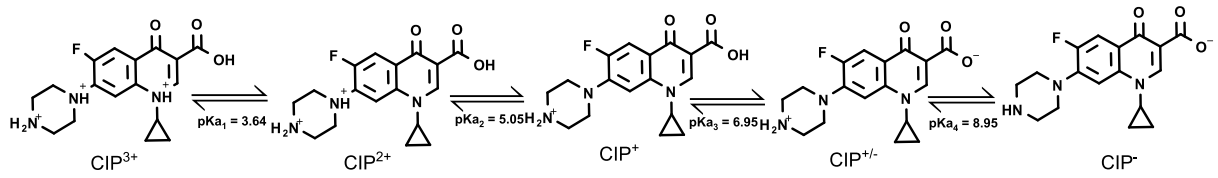

Fig. 5: Distribution of CIP, adapted from A. Salma *et al. (2016)* (Salma et al., 2016). Made in MarvinSketch (version 20.9).

Under acidic conditions, the protonated forms of CIP are predominant (CIP^{3+}, CIP^{2+} and CIP^{1+}). The degree of protonation decreases with increasing pH. Around pH 7-8, CIP is present in its neutral/zwitterionic form (CIP^{0}) and under alkaline solutions, CIP exists in its deprotonated form (CIP^{-1}). It is important to note that a change in CIP ionization state (or a change in pH) influences both the direct UV photolysis and the SR-AOP/ARP degradation experiments. Some ionization states of CIP are more prone to direct photolysis, while others are less affected. In a comparative study by Wammer *et al*. (2013), it was found that fluoroquinolone compounds (norfloxacin, ofloxacin and enrofloxacin) showed similar direct photolysis degradation kinetics at different pH values: the highest observed reaction rate constant was observed for the neutral form of the target molecules, followed by the deprotonated form and the protonated form (Wammer et al., 2013). This ranking is in accordance with the authors' results for direct UV photolysis of ciprofloxacin as shown in Figs. 6 and 7.

For the ARP experiments, the k_{obs} of the CIP degradation for pH values of 3, 6, 8.5 (non-adjusted pH) and 10 have been determined and results for both direct UV photolysis ($k_{obs,UV\ only}$) and the UV/sulfite process ($k_{obs,UV/sulfite}$) are shown in Fig. 6. From this figure, it is obvious that direct UV photolysis already partially contributes to CIP degradation in the UV/sulfite process, the results at pH 3 excluded. The obtained k_{obs} at pH 3 for both the direct UV

photolysis and the UV/sulfite process are low (k_{obs}=0 for direct photolysis and only 0.0108 min^{-1} for the UV/sulfite process). Increasing the pH value from 3 to 8.5 results in a proportional improvement of the removal rates ($k_{obs\ UV/sulfite}$ increases from 0.0108 to 0.269 min^{-1}). However, when further increasing the pH from 8.5 to 10, the CIP removal decreases, accompanied by a drop in the rate constants ($k_{obs,UV\ only}$ decreases from 0.106 to 0.0677 min^{-1} and $k_{UV/sulfite}$ decreases from 0.269 to 0.239 min^{-1}). For both the direct photolysis and the UV/sulfite process, the drop in k_{obs} is similar. These results suggest that the observed drop in k_{obs} for UV/sulfite at pH 10 is due to the lower affinity for direct photolysis of the ionized CIP form at pH 10.

The influence of pH on the UV/sulfite process for the degradation of CIP manifests itself in two ways: (*i*) the pH-dependent distribution of sulfite, resulting in the generation of different reducing radicals (e.g., $\bullet e_{aq}^-$ and •H) (Liu et al., 2013a; Xie et al., 2017) and (*ii*) the pH-dependent distribution of CIP: the produced radicals can have different affinities for the different ionization states of CIP (Ao et al., 2018; Salma et al., 2016).

Few literature sources have investigated the influence of pH for the removal of CIP using ARP processes. However, it has been reported that the deprotonation of the amine groups at the piperazine ring of CIP promotes the electron donating character of the CIP molecule and decreases the steric hindrance of CIP (Wei et al., 2013). Hence, when increasing the pH from 3 to 8, the degree of protonation of CIP diminishes from CIP^{3+} to CIP^{+}, which is beneficial for the attacks by $\bullet e_{aq}^-$. At pH 10, CIP is mainly present in its deprotonated form (CIP^{-1}), and $\bullet e_{aq}^-$ is expected to be the dominant radical in the system. As previously explained, the decrease in k_{obs} at this pH value can be attributed to a decrease in k_{obs} for direct photolysis of CIP. This was confirmed by Sarkhosh *et al*. (2019), who investigated the influence of the pH on the degradation of CIP using the UV/I^- process (in which $\bullet e_{aq}^-$ are the main reactive species produced), and found that this process was pH independent (Sarkhosh et al., 2019).

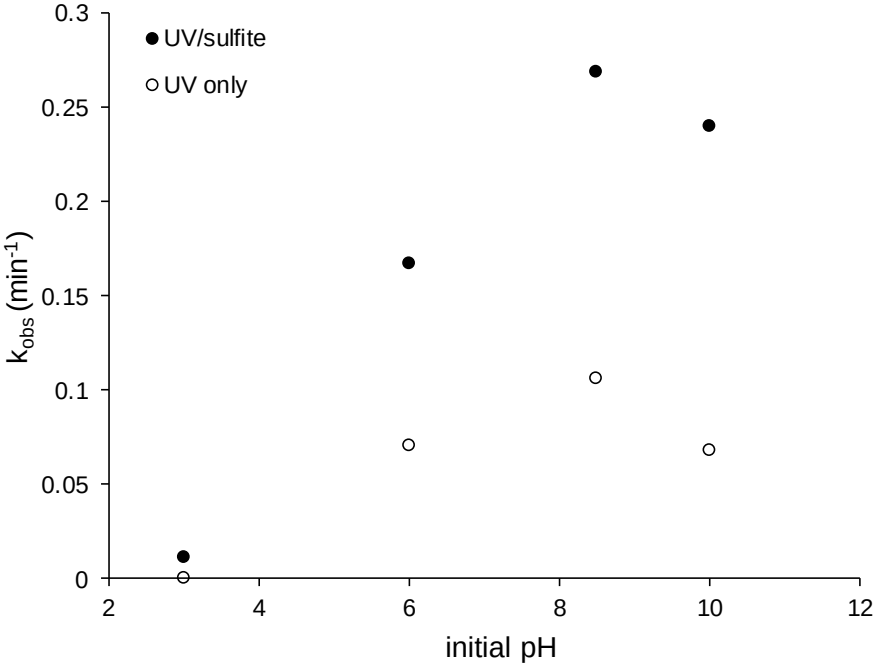

Fig. 6: Observed reaction rate constants (k_{obs}) in the UV/sulfite process as a function of initial pH values. Conditions: $[CIP]_0$ = 60.42 µM, $[SO_3^{2-}]_0$ = 1 mM, UV power = 18 W.

For the SR-AOP degradation experiments investigating the influence of pH, experiments were performed at initial pH values of 3, 6 (non-adjusted pH), 8 and 10. The resulting k_{obs} are shown in Fig. 7. A clear enhancement of the k_{obs} can be observed when PS is added to the reaction system (k_{obs} obtained at pH 6 for direct photolysis is 0.0703 min^{-1} and increases more than 10-fold when PS is added (k_{obs}=0.752 min^{-1}). For the UV/PS experiments, k_{obs} increases with increasing pH (an increase from 0.637 min^{-1}- 0.897 min^{-1} in the pH range of 3-8, respectively), and decreases at pH 10 (k_{obs} decreases to 0.792 min^{-1}). This can be attributed to (*i*) the pH-dependent generation of •OH in the system and (*ii*) similar to the UV/sulfite process, the produced radicals can have different affinities towards reaction with the different ionization forms of CIP. Following the results shown in Fig. 7, a maximal k_{obs} of 0.897 min^{-1} is obtained at pH 8. The reactive species thus have a higher affinity for the neutral form of CIP. The observed trend of k_{obs} with changing pH is in contrast with the results of Yang *et al.* (2019), who found an increase in k_{obs} in the pH range of 3-7, but a decrease in the pH range of 7-11

(Yang et al., 2019). Guo *et al.* (2017) had similar results to ours for the degradation of similar fluoroquinolones, but found an increase in k_{obs} in the pH range of 3-9, and only observed a drop in k_{obs} at a pH of 11 (Guo et al., 2017). In the investigated pH range (3-10) this is more in agreement with the authors' results.

To obtain a clearer insight in the reactive species present in both the UV/sulfite and the UV/PS process, the radical contributions at different pH were investigated in the next section. This enables a more in-depth elucidation of the pH-dependent degradation efficiency.

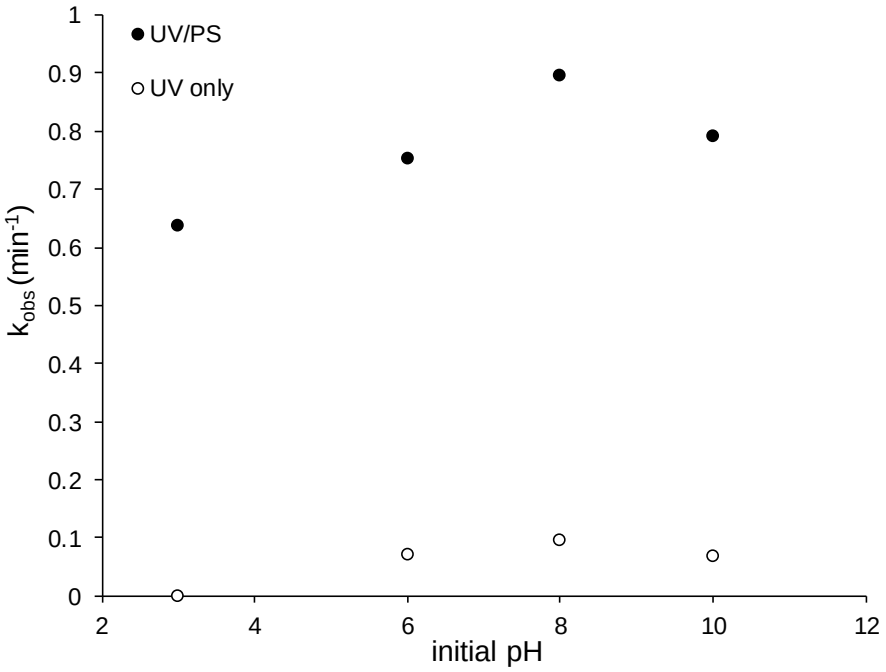

Fig. 7: Observed reaction rate constants (k_{obs}) in the UV/PS process as a function of initial pH values. Conditions: $[CIP]_0$ = 60.42 µM, $[PS]_0$ = 1.1 mM, UV power = 18 W.

3.5 Radical contributions

Radical scavenging experiments were carried out to investigate the contribution of the different reactive species formed in both the UV/sulfite and the UV/PS process. For the UV/sulfite process, the main reactive species are $\bullet e_{aq}^-$ and •H, whereas in the UV/PS process, the main reactive species are $\bullet SO_4^-$ and •OH.

In the UV/sulfite process, nitrate (NO_3^-) and t-butanol (TBA) were used as radical scavengers. It has been reported that nitrate is a good scavenger for both $\bullet e_{aq}^-$ and •H (Eq. (7) and (8)) (Xiao et al., 2017a), while t-butanol only quenches •H (Eq. (9)) (Hardison et al., 2002).

$$NO_3^- + \bullet e_{aq}^- \rightarrow (\bullet NO_3)^{2-} \qquad (k = 9.7 \times 10^9\ M^{-1}\ s^{-1}) \qquad (7)$$

$$NO_3^- + \bullet H \rightarrow (NO_3H \bullet)^- \qquad (k = 1.4 \times 10^6\ M^{-1}\ s^{-1}) \qquad (8)$$

$$(CH_3)_3COH + \bullet H \rightarrow \bullet CH_2(CH_3)_2COH + H_2 \qquad (k = 1.7 \times 10^5\ M^{-1}\ s^{-1}) \qquad (9)$$

Under weakly alkaline and acidic conditions, the introduction of NO_3^- resulted in a significant inhibition in CIP removal. Upon addition of NO_3^-, the observed reaction rate constants were similar to those obtained under direct UV photolysis ($k_{obs,UV\ only}$ = 0.104 min^{-1} compared to $k_{obs,nitrate}$= 0.118 min^{-1}). This reveals the essential role of the reducing radicals in the improvement of CIP degradation relative to the direct UV photolytic process.

Li *et al.* (2012) have reported that sulfite exists in a monoanionic form (HSO_3^-) at pH ≤ 6 and in a dianionic form (SO_3^{2-}) at pH ≥ 8 (Li et al., 2012). Both forms co-exist in the pH range 6-8. As previously mentioned (Eqs. (3) and (4)), the presence of SO_3^{2-} contributes to the formation of $\bullet e_{aq}^-$, whereas HSO_3^- is the precursor of •H formation.

To further distinguish between the contribution of $\bullet e_{aq}^-$ and •H at different initial pH conditions, the relative contribution of both reactive species and their contribution to the k_{obs} in the UV/sulfite process was calculated using following equations:

$$\bullet H(\%) = \frac{k_{obs,UV/sulfite} - k_{obs,TBA}}{k_{obs,UV/sulfite} - k_{obs,NO_3^-}} \qquad k_{obs,\bullet H} = \left(k_{obs} - k_{obs,UV}\right) \times \bullet H(\%) \qquad (10)$$

$$\bullet e_{aq}^-(\%) = 100\% - \bullet H(\%) \qquad k_{obs,\bullet e_{aq}^-} = \left(k_{obs} - k_{obs,UV}\right) \times \bullet e_{aq}^-(\%) \qquad (11)$$

Considering these equations, 19% of the radical-dependent CIP degradation can be attributed to •H at pH 8.5, while 81% can be attributed to degradation by $\bullet e_{aq}^-$. Decreasing the pH to a

value of 6.0 leads to an increase in •H contribution to 58% and, correspondingly, a decrease in contribution of $•e_{aq}^-$ to 42%. Fig. 8 shows the contributions of direct UV photolysis, $•e_{aq}^-$ and •H to the k_{obs} in the UV/sulfite process at different pH values. This figure shows the increase in $•e_{aq}^-$ contribution with increasing pH, confirming the promoted production of $•e_{aq}^-$ when the sulfite ion is present in its dianionic form (SO_3^{2-}). Next to this, according to Eq. (12), •H can be converted into $•e_{aq}^-$ in alkaline solutions. As a result, $•e_{aq}^-$ was proven to be the responsible radical for CIP degradation (not taking into account direct UV photolysis) at strong alkaline conditions. Under acidic conditions (pH 3.0), no contribution of $•e_{aq}^-$ was found and •H is the predominant radical. However, although •H is formed, the degradation of CIP is not to a similar extent as when $•e_{aq}^-$ is predominant. This could be explained by the low reaction rate of •H with CIP in its triplet state (CIP^{3+}). Therefore, the degradation of CIP in the UV/sulfite process is most favorable in neutral and alkaline conditions.

$$• H + OH^- \rightarrow • e_{aq}^- + H_2O \qquad (k = 2.2\times10^7\ M^{-1}s^{-1}) \qquad (12)$$

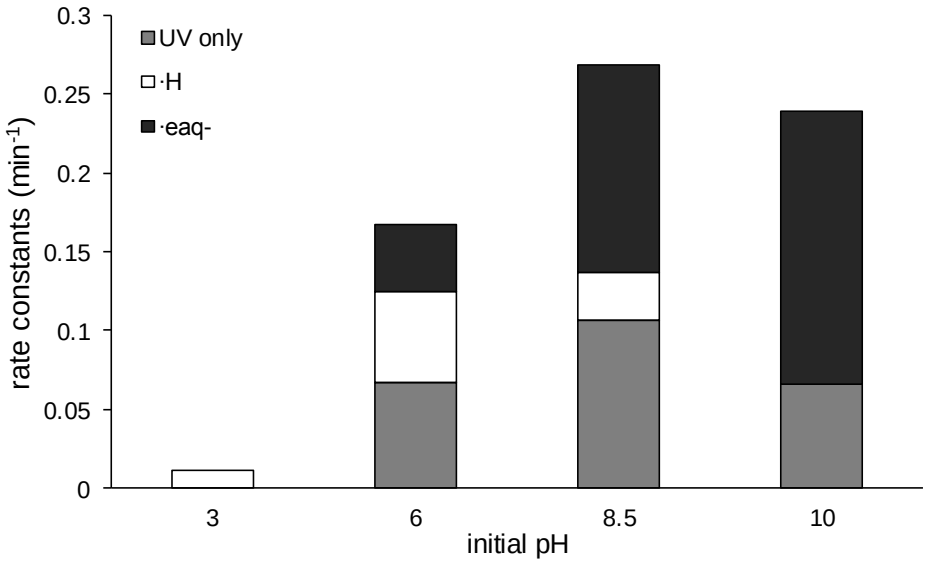

Fig. 8: Relative contributions of $•e_{aq}$-, •H, and UV only in the UV/sulfite process

Conditions: $[CIP]_0$ = 60.42 µM, $[SO_3^{2-}]_0$ = 1.0 mM, UV power = 18 W.

For the UV/PS system, radical scavenging experiments were conducted as follows: to scavenge both •OH and $•SO_4^-$, ethanol (EtOH) was added to the reaction mixture due to its high reaction rate constants with both •OH and $•SO_4^-$. To be able to distinguish between •OH and $•SO_4^-$, t-butanol (TBA) was added to the reaction mixture, due to its high reaction rate constant with •OH and relatively low reaction rate constant with $•SO_4^-$. The contributions of •OH and $•SO_4^-$ can then, in a similar way to the UV/sulfite process, be expressed as shown in Eqs. (13) and (14), respectively.

$$\bullet OH\ (\%) = \frac{k_{obs,ref} - k_{obs,TBA}}{k_{obs,ref} - k_{obs,EtOH}} \qquad k_{obs,\bullet OH} = \left(k_{obs} - k_{obs,UV}\right) \times \bullet OH(\%) \quad (13)$$

$$\bullet SO_4^-(\%) = 100\% - \bullet OH(\%) \qquad k_{obs,\bullet SO_4^-} = \left(k_{obs} - k_{obs,UV}\right) \times \bullet SO_4^-(\%) \quad (14)$$

The contribution of both •OH and $•SO_4^-$ was calculated for different initial pH values to confirm the presence of •OH. The results are shown in Fig. 9 (due to the limited difference between $k_{obs,ref}$, $k_{obs,TBA}$ and $k_{obs,EtOH}$ at pH 10, no distinction in •OH/$•SO_4^-$ contribution was made for pH 10). Despite the hypothesis of Eq. (1), which states that two $•SO_4^-$ are produced for every PS molecule, about 33% of the radical species at an initial pH of 3 are distinguished to be •OH. The •OH percentage increases with increasing pH with an abundance of 65% at pH 8. This is in contradiction with previous findings, where the heat activated PS process was investigated and it was found that no (or very little) •OH was present in this reaction system (in thermal activation, radicals are produced in a similar way as in UV activation) (Milh et al., 2020).

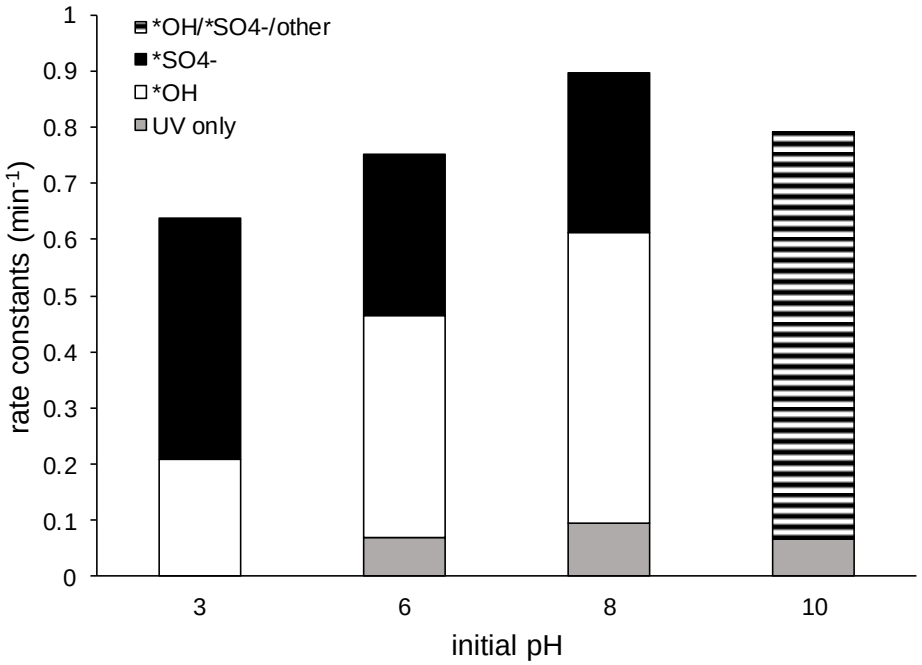

Fig. 9: Relative contributions of •OH, $•SO_4^-$ and UV only in the UV/PS process

Conditions: $[CIP]_0$ = 60.42 µM, $[PS]_0$ = 1.1 mM, UV power = 18 W.

Possible explanations for the presence of •OH can be found in Eqs. (15) and (16) (Ji et al., 2015).

$$• SO_4^- + OH^- \rightarrow SO_4^{2-} + • OH \qquad (k = 6.5 \times 10^7\ M^{-1}\ s^{-1}) \qquad (15)$$

$$• SO_4^- + H_2O \rightarrow SO_4^{2-} + • OH + H^+ \qquad (k < 3 \times 10^3\ M^{-1}\ s^{-1}) \qquad (16)$$

Eq. (15) shows that a conversion of $•SO_4^-$ to •OH is possible in alkaline conditions (due to the availability to react with hydroxide ions). However, the formation of •OH as stated in this equation, is said to be predominant at pH>9 (Oh et al., 2016). At a pH of 10, the contribution of •OH is thus expected to increase even more relatively to pH 8. However, this does not explain the contribution of •OH at neutral and acidic pH.

An explanation for the occurrence of •OH in neutral and acidic conditions can be found in Eq. (16). This equation shows the production of •OH through hydrolysis of $•SO_4^-$ and has a relatively low reaction rate constant. The heat-activated PS process is characterized by a relatively slow PS consumption, whereas the PS consumption in the UV/PS is much faster. This

454 results in a (relatively) high $\bullet SO_4^-$ concentration in the UV/PS system, increasing the possibility
455 of Eq. (16) to take place. In the heat-activated PS process, the $\bullet SO_4^-$ concentration is relatively
456 low, so any $\bullet SO_4^-$ produced in the system will immediately react with the target molecule,
457 because of its higher reaction rate constant with the molecule compared to the reaction rate of
458 Eq. (16). In the UV/PS process, the high $\bullet SO_4^-$ concentration results in an "excess" of $\bullet SO_4^-$
459 relative to the target molecule, so the $\bullet SO_4^-$ present undergoes a hydrolysis reaction and •OH is
460 produced. To confirm this hypothesis, thermal degradation experiments were conducted with
461 CIP at similar conditions as the experiments performed in the UV/PS process. It was confirmed
462 that at a temperature of 70 °C, and with an $[PS]_0$ of 1.1 mM, only 6% of the initial PS
463 concentration was consumed in a reaction time of 30 min. This is in contrast with the results
464 obtained for the UV/PS process, where 53% of PS was consumed at an $[PS]_0$ of 1 mM and in a
465 reaction time 40 min. By conducting radical scavenging experiments for both processes, it was
466 shown that at non-adjusted pH, only 8% of the produced radicals were •OH for the heat-
467 activated PS process, in contrast to 58% for the UV/PS process. This could explain the
468 formation of •OH in the UV/PS process.

469 Thus, both $\bullet SO_4^-$ and •OH play a role in CIP degradation in the UV/PS process. The affinity of
470 both radicals for the different ionization states of CIP (depending on the pH) is a crucial
471 parameter to obtain an optimal CIP degradation. In the literature, $\bullet SO_4^-$ was found to be
472 vulnerable for reaction with the protonated piperazine group of CIP, which can contribute to
473 the high k_{obs} at neutral pH (Guo et al., 2017). Also at neutral pH, it was found that the CIP
474 degradation efficiency using the UV/H_2O_2 process (where only •OH is produced) is lower
475 compared to the UV/PS process (Yang et al., 2019). This highlights the importance of $\bullet SO_4^-$ in
476 this process. Following this hypothesis, as a decrease in k_{obs} at lower pH (higher $\bullet SO_4^-$
477 production) is observed, it can be assumed that the affinity of $\bullet SO_4^-$ is smaller for the ionization
478 states of CIP with a higher protonation degree. Sun *et al.* (2019) have reported that for ofloxacin

(a structurally related fluoroquinolone compound), the increase in protonation can cause a higher resistance towards reactions with electrophilic compounds (such as $\bullet SO_4^-$), which could confirm this (Sun et al., 2019).

At pH 10, no increase in degradation efficiency is observed. This can be explained by a change in CIP distribution (from the zwitterionic to the anionic form) and therefore, a change in affinity of the radicals for this form (as the piperazine group is deprotonated in this ionization form, reaction with $\bullet SO_4^-$ is less likely). In general, the reaction of •OH (which is the predominant radical at this pH) with organic molecules is less selective, which can explain why a significant degradation is still observed (Khan et al., 2017). Additionally, Yang *et al.* (2019) have reported a decrease in the oxidation potential of •OH at higher pH, which can also be the cause of this decrease (Yang et al., 2019). It can be concluded that, although $\bullet SO_4^-$ is not the predominant radical at the conditions where maximal CIP degradation efficiency is observed, it plays a major role in the CIP degradation.

3.6 Defluorination efficiency

As previously mentioned, one of the most essential differences between AOPs and ARPs is the dehalogenation efficiency of the respective processes. This dehalogenation efficiency is of specific interest, considering that dehalogenation often leads to the formation of less toxic and biodegradable degradation products (Gaurav and Bharagava, 2020). Furthermore, the dehalogenation efficiency profiles of the respective processes (and most importantly the dissimilarities between the two profiles) can provide insight in the difference in reaction mechanisms of reducing and oxidizing radicals. Hence, the release of fluorine atoms from the CIP molecule as fluoride ions (F^-) in both the UV/PS and the UV/sulfite process was investigated. Fig. 10 shows the obtained defluorination efficiency for the UV/PS and the UV/sulfite process. The defluorination efficiency is defined as the fluoride concentration

divided by the maximum fluoride concentration (this was calculated corresponding to the initial CIP concentration).

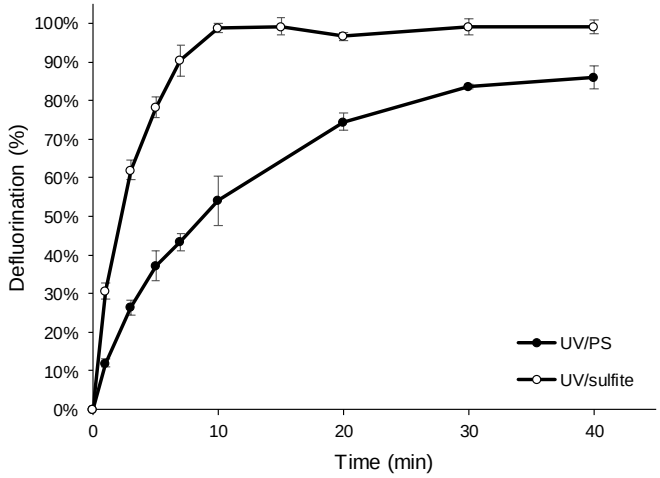

Fig. 10: Defluorination efficiency of the UV/PS and UV/sulfite process

Conditions: $[CIP]_0$ = 60.42 µM, $pH_{UV/sulfite}$= 8.5 and $pH_{UV/PS}$= 8, $[PS]_0$ =$[Sulfite]_0$ = 1.0 mM, UV power = 18 W.

For the UV/PS process, a defluorination efficiency of 86% is obtained within 40 min, which reveals its ability to attack the C-F bond of the CIP molecule. However, no full defluorination is observed and residual fluorinated compounds are still present in the system. For the UV/sulfite process, a defluorination efficiency of 99% is obtained in the same reaction time and reaction conditions, indicating an almost complete cleavage of C-F bonds during the process. Although the UV/PS process can degrade CIP much faster than the UV/sulfite process (96% degradation for the UV/PS process and 89% degradation for the UV/sulfite process in 7 min reaction time), the defluorination efficiency does not follow this trend (43% for the UV/PS process and 89% for the UV/sulfite process), revealing their different mechanisms of action. During the UV/sulfite process, the primary degradation path of CIP degradation is through the breakage of the C-F bonds, caused by the strong dehalogenation properties of the produced reducing radicals. The dehalogenation capability of the UV/sulfite process was confirmed by Li *et al.* (2012), who reported an efficient dechlorination of monochloroacetic acid (MCAA) by

523 the UV/sulfite process, mainly induced by $\bullet e_{aq}^-$ (Li et al., 2012). For the UV/PS process,
524 however, dehalogenation is proposed not to be the major pathway in the degradation of
525 halogenated compounds: Hou *et al.* (2017) confirmed this for the degradation of
526 haloacetonitriles (Hou et al., 2017). For the degradation of CIP, Mahdi-Ahmed *et al.* (2014)
527 and Guo *et al*. (2016), who investigated the UV/PMS and the heat/PS process (in which similar
528 radicals are produced), respectively, found similar results (Guo et al., 2016; Mahdi-Ahmed and
529 Chiron, 2014).

530 To further prove this conclusion, the total fluoride (TF) concentration ($[TF]_t$) was calculated as
531 the sum of the free fluoride ions ($[F^-]_t$) and the available fluorine atoms in the residual CIP
532 molecules ($[CIP]_t$) at defined time intervals. A relative TF value for each time point is then
533 obtained by dividing the obtained TF value ($[TF]_t$) by the initial TF value ($[TF]_0$) as shown in
534 Eq. (17).

535 $$relative\ TF\ value\ (\%) = \frac{[TF]_t}{[TF]_0} = \frac{[F^-]_t + [CIP]_t}{[F^-]_0 + [CIP]_0} \quad (17)$$

536 The calculation of the relative TF value enables to elucidate the formation of fluorinated
537 degradation products: when the relative TF value is close to 100%, the F atom is directly
538 removed from the CIP molecule, and a decrease of $[CIP]_t$ leads to a direct increase of $[F^-]_t$.
539 When fluorinated degradation products are formed, $[CIP]_t$ decreases, but an increase in $[F^-]$ is
540 not detected. The results of the relative TF value calculation for both processes are shown in
541 Fig. 11. For the UV/sulfite process, the relative TF value is close to 100% during the entire
542 reaction process. This shows that the fluorine atom is almost immediately released from the
543 CIP molecule and transformed into free fluoride ions. For the UV/PS process, the relative TF
544 value is much lower in the first stage of the process and then gradually increases, revealing the
545 formation of F-containing intermediates during the degradation process.

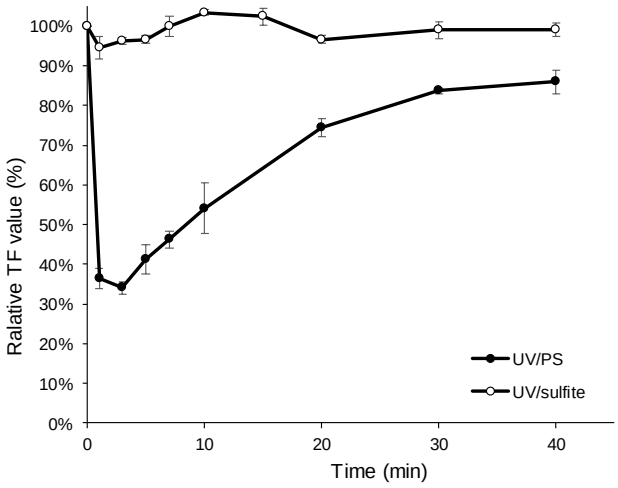

Fig. 11: Relative TF value for the UV/PS and UV/sulfite process

Conditions: $[CIP]_0$ = 60.42 µM, non-adjusted pH, $[PS]_0$ = $[Sulfite]_0$ = 1.0 mM, UV power = 18 W.

4. Conclusion

The aim of this study was to compare UV-based SR-AOP and ARP processes for the removal of the antibiotic compound ciprofloxacin (CIP) from (waste)water. Firstly, the UV/PS process was found to be the most efficient among the UV-based SR-AOPs (complete removal after a reaction time of 10 mins), while the UV/sulfite process was the most efficient for the ARPs (complete removal after a reaction time of 20 mins) under the same reaction conditions. Thereafter, the process parameters were optimized for both processes. It was found that for both processes, the removal efficiency increased with increasing initial oxidant/reductant concentration, however, this increase stagnated at higher concentrations. Increasing the UV intensity also led to higher removal efficiencies for both processes. A slightly alkaline pH was found to result in the highest degradation efficiency for both the UV/PS (k_{obs}=0.897 min^{-1}) and the UV/sulfite process (k_{obs}=0.269 min^{-1}). For the UV/PS process, it was found that the produced reactive species at pH 8 (which were found to be both •OH and $•SO_4^-$) were more prone to react with the ionization state of CIP at that pH (neutral form). For the UV/sulfite process, $•e_{aq}^-$ was found to be most reactive towards CIP. At non-adjusted pH (pH 8.5), the

production of $\bullet e_{aq}^-$ was found to be the highest, resulting in a maximal degradation efficiency of CIP.

In general, the UV/PS process was found to be much more efficient in removing CIP than the UV/sulfite process (at optimized conditions, the k_{obs} for the UV/PS process was found to be approximately three times higher than the k_{obs} for the UV/sulfite process). However, even though higher CIP degradation rates were obtained using the UV/PS process, it was found that the UV/sulfite process was much more efficient in the defluorination of CIP.

5. Acknowledgements

Hannah Milh holds a PhD fellowship awarded by the Research Foundation – Flanders (FWO) [grant number 11D7418N]. Xingyue Yu holds a PhD grant awarded by the China Scholarship Council (CSC) [grant number 201606200054]. The Private Foundation De Nayer is kindly thanked for providing the Methrohm 883 Basic IC Plus Ion Chromatograph.

6. References

Ao, X., Liu, W., Sun, W., Cai, M., Ye, Z., Yang, C., Lu, Z., Li, C., 2018. Medium pressure UV-activated peroxymonosulfate for ciprofloxacin degradation: Kinetics, mechanism, and genotoxicity. Chem. Eng. J. 345, 87–97. https://doi.org/10.1016/j.cej.2018.03.133

Boczkaj, G., Fernandes, A., 2017. Wastewater treatment by means of advanced oxidation processes at basic pH conditions: A review. Chem. Eng. J. https://doi.org/10.1016/j.cej.2017.03.084

Caliman, F.A., Gavrilescu, M., 2009. Pharmaceuticals, personal care products and endocrine disrupting agents in the environment - A review. Clean - Soil, Air, Water 37, 277–303. https://doi.org/10.1002/clen.200900038

Dewil, R., Mantzavinos, D., Poulios, I., Rodrigo, M.A., 2017. New perspectives for Advanced

587 Oxidation Processes. J. Environ. Manage. 195, 93–99.
588 https://doi.org/10.1016/j.jenvman.2017.04.010

589 Ebele, A.J., Abou-Elwafa Abdallah, M., Harrad, S., 2017. Pharmaceuticals and personal care
590 products (PPCPs) in the freshwater aquatic environment. Emerg. Contam. 3, 1–16.
591 https://doi.org/10.1016/j.emcon.2016.12.004

592 Fedorov, K., Plata-Gryl, M., Khan, J.A., Boczkaj, G., 2020. Ultrasound-assisted heterogeneous
593 activation of persulfate and peroxymonosulfate by asphaltenes for the degradation of
594 BTEX in water. J. Hazard. Mater. 397. https://doi.org/10.1016/j.jhazmat.2020.122804

595 Fekadu, S., Alemayehu, E., Dewil, R., Van Der Bruggen, B., 2019. Pharmaceuticals in
596 freshwater aquatic environments: A comparison of the African and European challenge.
597 Sci. Total Environ. 654, 324–337. https://doi.org/10.1016/j.scitotenv.2018.11.072

598 Gadipelly, C., Pérez-González, A., Yadav, G.D., Ortiz, I., Ibáñez, R., Rathod, V.K., Marathe,
599 K. V, 2014. Pharmaceutical Industry Wastewater: Review of the Technologies for Water
600 Treatment and Reuse. Ind. Eng. Chem. Res. 53, 11571–11592.
601 https://doi.org/10.1021/ie501210j

602 García-Galán, M.J., Anfruns, A., Gonzalez-Olmos, R., Rodriguez-Mozaz, S., Comas, J., 2016.
603 Advanced oxidation of the antibiotic sulfapyridine by UV/H2O2: Characterization of its
604 transformation products and ecotoxicological implications. Chemosphere 147, 451–459.
605 https://doi.org/10.1016/j.chemosphere.2015.12.108

606 Gaurav, S., Bharagava, R.N., 2020. Bioremediation of Industrial Waste for Environmental
607 Safety, Bioremediation of Industrial Waste for Environmental Safety. Springer Singapore.
608 https://doi.org/10.1007/978-981-13-1891-7

609 Ghanbari, F., Moradi, M., 2017. Application of peroxymonosulfate and its activation methods

for degradation of environmental organic pollutants: Review. Chem. Eng. J. https://doi.org/10.1016/j.cej.2016.10.064

Guo, H., Gao, N., Yang, Y., Zhang, Y., 2016. Kinetics and transformation pathways on oxidation of fluoroquinolones with thermally activated persulfate. Chem. Eng. J. 292, 82–91. https://doi.org/10.1016/j.cej.2016.01.009

Guo, H., Ke, T., Gao, N., Liu, Y., Cheng, X., 2017. Enhanced degradation of aqueous norfloxacin and enrofloxacin by UV-activated persulfate: Kinetics, pathways and deactivation. Chem. Eng. J. 316, 471–480. https://doi.org/10.1016/j.cej.2017.01.123

Hardison, D.R., Cooper, W.J., Mezyk, S.P., Bartels, D.M., 2002. The free radical chemistry of tert-butyl formate: Rate constants for hydroxyl radical, hydrated electron and hydrogen atom reaction in aqueous solution. Radiat. Phys. Chem. 65, 309–315. https://doi.org/10.1016/S0969-806X(02)00333-X

Hou, S., Ling, L., Shang, C., Guan, Y., Fang, J., 2017. Degradation kinetics and pathways of haloacetonitriles by the UV/persulfate process. Chem. Eng. J. 320, 478–484. https://doi.org/10.1016/j.cej.2017.03.042

Ji, Y., Fan, Y., Liu, K., Kong, D., Lu, J., 2015. Thermo activated persulfate oxidation of antibiotic sulfamethoxazole and structurally related compounds. Water Res. 87, 1–9. https://doi.org/10.1016/j.watres.2015.09.005

Johnson, A.C., Keller, V., Dumont, E., Sumpter, J.P., 2015. Assessing the concentrations and risks of toxicity from the antibiotics ciprofloxacin, sulfamethoxazole, trimethoprim and erythromycin in European rivers. Sci. Total Environ. 511, 747–755. https://doi.org/10.1016/j.scitotenv.2014.12.055

Jung, B., Farzaneh, H., Khodary, A., Abdel-Wahab, A., 2015. Photochemical degradation of

633 trichloroethylene by sulfite-mediated UV irradiation. J. Environ. Chem. Eng. 3, 2194–
634 2202. https://doi.org/10.1016/j.jece.2015.07.026

635 Kamel, D., Sihem, A., Halima, C., Tahar, S., 2009. Decolourization process of an azoïque dye
636 (Congo red) by photochemical methods in homogeneous medium. Desalination 247, 412–
637 422. https://doi.org/10.1016/j.desal.2009.02.052

638 Kanjal, M.I., Muneer, M., Abdelhaleem, A., Chu, W., 2020. Degradation of methotrexate by
639 UV/Peroxymonosulphate: Kinetics, effect of operational parameters and mechanism.
640 Chinese J. Chem. Eng. https://doi.org/10.1016/j.cjche.2020.05.033

641 Khan, S., He, X., Khan, J.A., Khan, H.M., Boccelli, D.L., Dionysiou, D.D., 2017. Kinetics and
642 mechanism of sulfate radical-and hydroxyl radical-induced degradation of highly
643 chlorinated pesticide lindane in UV/peroxymonosulfate system. Chem. Eng. J. 318, 135–
644 142. https://doi.org/10.1016/j.cej.2016.05.150

645 Kim, S., Chu, K.H., Al-Hamadani, Y.A., Park, C.M., Jang, M., Kim, D.H., Yu, M., Heo, J.,
646 Yoon, Y., 2018. Removal of contaminants of emerging concern by membranes in water
647 and wastewater: A review. Chem. Eng. J. 335, 896–914.
648 https://doi.org/10.1016/j.cej.2017.11.044

649 Li, X., Ma, J., Liu, G., Fang, J., Yue, S., Guan, Y., Chen, L., Liu, X., 2012. Efficient reductive
650 dechlorination of monochloroacetic acid by sulfite/UV process. Environ. Sci. Technol. 46,
651 7342–7349. https://doi.org/10.1021/es3008535

652 Lin, C.C., Wu, M.S., 2014. Degradation of ciprofloxacin by UV/S2O82- process in a large
653 photoreactor. J. Photochem. Photobiol. A Chem. 285, 1–6.
654 https://doi.org/10.1016/j.jphotochem.2014.04.002

655 Liu, X., Yoon, S., Batchelor, B., Abdel-Wahab, A., 2013a. Photochemical degradation of vinyl

chloride with an Advanced Reduction Process (ARP) - Effects of reagents and pH. Chem. Eng. J. 215–216, 868–875. https://doi.org/10.1016/j.cej.2012.11.086

Liu, X., Yoon, S., Batchelor, B., Abdel-Wahab, A., 2013b. Degradation of vinyl chloride (VC) by the sulfite/UV advanced reduction process (ARP): Effects of process variables and a kinetic model. Sci. Total Environ. 454–455, 578–583. https://doi.org/10.1016/j.scitotenv.2013.03.060

Luo, C., Jiang, J., Ma, J., Pang, S., Liu, Y., Song, Y., Guan, C., Li, J., Jin, Y., Wu, D., 2016. Oxidation of the odorous compound 2,4,6-trichloroanisole by UV activated persulfate: Kinetics, products, and pathways. Water Res. 96, 12–21. https://doi.org/10.1016/j.watres.2016.03.039

Mahdi-Ahmed, M., Chiron, S., 2014. Ciprofloxacin oxidation by UV-C activated peroxymonosulfate in wastewater. J. Hazard. Mater. 265, 41–46. https://doi.org/10.1016/j.jhazmat.2013.11.034

Mayhew, S.G., 1978. The Redox Potential of Dithionite and SO−2 from Equilibrium Reactions with Flavodoxins, Methyl Viologen and Hydrogen plus Hydrogenase. Eur. J. Biochem. 85, 535–547. https://doi.org/10.1111/j.1432-1033.1978.tb12269.x

Melsheimer, J., Schlögl, R., 1997. Identification of reaction products of mild oxidation of H2S in solution and in solid state by UV-VIS spectroscopy. Fresenius. J. Anal. Chem. 357, 397–400. https://doi.org/10.1007/s002160050177

Mezzelani, M., Gorbi, S., Regoli, F., 2018. Pharmaceuticals in the aquatic environments: Evidence of emerged threat and future challenges for marine organisms. Mar. Environ. Res. 140, 41–60. https://doi.org/10.1016/j.marenvres.2018.05.001

Milh, H., Schoenaers, B., Stesmans, A., Cabooter, D., Dewil, R., 2020. Degradation of

679 sulfamethoxazole by heat-activated persulfate oxidation: Elucidation of the degradation
680 mechanism and influence of process parameters. Chem. Eng. J. 379, 122–234.
681 https://doi.org/10.1016/j.cej.2019.122234

682 Neta, P., Huie, R.E., 1985. Free-radical chemistry of sulfite. Environ. Health Perspect. VOL.
683 64, 209–217.

684 Oh, W. Da, Dong, Z., Lim, T.T., 2016. Generation of sulfate radical through heterogeneous
685 catalysis for organic contaminants removal: Current development, challenges and
686 prospects. Appl. Catal. B Environ. https://doi.org/10.1016/j.apcatb.2016.04.003

687 Petrie, B., Barden, R., Kasprzyk-Hordern, B., 2014. A review on emerging contaminants in
688 wastewaters and the environment: Current knowledge, understudied areas and
689 recommendations for future monitoring. Water Res. 72, 3–27.
690 https://doi.org/10.1016/j.watres.2014.08.053

691 Ran, G., Li, Q., 2020. Degradation of refractory organic compounds from dinitrodiazophenol
692 containing industrial wastewater through UV/H2O2 and UV/PS processes. Environ. Sci.
693 Pollut. Res. 27, 6042–6051. https://doi.org/10.1007/s11356-019-07367-1

694 Salma, A., Thoröe-Boveleth, S., Schmidt, T.C., Tuerk, J., 2016. Dependence of transformation
695 product formation on pH during photolytic and photocatalytic degradation of
696 ciprofloxacin. J. Hazard. Mater. 313, 49–59.
697 https://doi.org/10.1016/j.jhazmat.2016.03.010

698 Sarkhosh, M., Sadani, M., Abtahi, M., Mohseni, S.M., Sheikhmohammadi, A., Azarpira, H.,
699 Najafpoor, A.A., Atafar, Z., Rezaei, S., Alli, R., Bay, A., 2019. Enhancing photo-
700 degradation of ciprofloxacin using simultaneous usage of eaq− and *OH over UV/ZnO/I-
701 process: Efficiency, kinetics, pathways, and mechanisms. J. Hazard. Mater. 377, 418–426.
702 https://doi.org/10.1016/j.jhazmat.2019.05.090

703 Sharma, J., Mishra, I.M., Kumar, V., 2015. Degradation and mineralization of Bisphenol A
704 (BPA) in aqueous solution using advanced oxidation processes: UV/H2O2 and
705 UV/S2O82- oxidation systems. J. Environ. Manage. 156, 266–275.
706 https://doi.org/10.1016/j.jenvman.2015.03.048

707 Somathilake, P., Dominic, J.A., Achari, G., Langford, C.H., Tay, J.H., 2019. Influence of UV
708 dose on the UV/H2O2 process for the degradation of carbamazepine in wastewater.
709 Environ. Technol. (United Kingdom) 40, 3031–3039.
710 https://doi.org/10.1080/09593330.2018.1464065

711 Sun, Y., Cho, D.W., Graham, N.J.D., Hou, D., Yip, A.C.K., Khan, E., Song, H., Li, Y., Tsang,
712 D.C.W., 2019. Degradation of antibiotics by modified vacuum-UV based processes:
713 Mechanistic consequences of H2O2 and K2S2O8 in the presence of halide ions. Sci. Total
714 Environ. 664, 312–321. https://doi.org/10.1016/j.scitotenv.2019.02.006

715 Taheran, M., Naghdi, M., Brar, S.K., Verma, M., Surampalli, R.Y., 2018. Emerging
716 contaminants: Here today, there tomorrow! Environ. Nanotechnology, Monit. Manag. 10,
717 122–126. https://doi.org/10.1016/j.enmm.2018.05.010

718 Van Doorslaer, X., Demeestere, K., Heynderickx, P.M., Langenhove, H. Van, Dewulf, J., 2011.
719 UV-A and UV-C induced photolytic and photocatalytic degradation of aqueous
720 ciprofloxacin and moxifloxacin: Reaction kinetics and role of adsorption 101, 540–547.
721 https://doi.org/10.1016/j.apcatb.2010.10.027

722 Wacławek, S., Lutze, H. V, Grübel, K., Padil, V.V., Černík, M., Dionysiou, D.D., 2017.
723 Chemistry of persulfates in water and wastewater treatment: A review. Chem. Eng. J. 330,
724 44–62. https://doi.org/10.1016/j.cej.2017.07.132

725 Wammer, K.H., Korte, A.R., Lundeen, R.A., Sundberg, J.E., McNeill, K., Arnold, W.A., 2013.
726 Direct photochemistry of three fluoroquinolone antibacterials: Norfloxacin, ofloxacin, and

727 enrofloxacin. Water Res. 47, 439–448. https://doi.org/10.1016/j.watres.2012.10.025

728 Wang, J., Wang, S., 2018. Activation of persulfate (PS) and peroxymonosulfate (PMS) and
729 application for the degradation of emerging contaminants. Chem. Eng. J.
730 https://doi.org/10.1016/j.cej.2017.11.059

731 Wei, X., Chen, J., Xie, Q., Zhang, S., Ge, L., Qiao, X., 2013. Distinct photolytic mechanisms
732 and products for different dissociation species of ciprofloxacin. Environ. Sci. Technol. 47,
733 4284–4290. https://doi.org/10.1021/es400425b

734 Xiao, Q., Wang, T., Yu, S., Yi, P., Li, L., 2017a. Influence of UV lamp, sulfur(IV)
735 concentration, and pH on bromate degradation in UV/sulfite systems: Mechanisms and
736 applications. Water Res. 111, 288–296. https://doi.org/10.1016/j.watres.2017.01.018

737 Xiao, Q., Yu, S., Li, L., Wang, T., Liao, X., Ye, Y., 2017b. An overview of advanced reduction
738 processes for bromate removal from drinking water: Reducing agents, activation methods,
739 applications and mechanisms, Journal of Hazardous Materials.
740 https://doi.org/10.1016/j.jhazmat.2016.10.053

741 Xie, B., Li, X., Huang, X., Xu, Z., Zhang, W., Pan, B., 2017. Enhanced debromination of 4-
742 bromophenol by the UV/sulfite process: Efficiency and mechanism. J. Environ. Sci.
743 (China) 54, 231–238. https://doi.org/10.1016/j.jes.2016.02.001

744 Xie, P., Ma, J., Liu, W., Zou, J., Yue, S., Li, X., Wiesner, M.R., Fang, J., 2015. Removal of 2-
745 MIB and geosmin using UV/persulfate: Contributions of hydroxyl and sulfate radicals.
746 Water Res. 69, 223–233. https://doi.org/10.1016/j.watres.2014.11.029

747 Yang, H., Li, Y., Chen, Y., Ye, G., Sun, X., 2019. Comparison of ciprofloxacin degradation in
748 reclaimed water by UV/chlorine and UV/persulfate advanced oxidation processes. Water
749 Environ. Res. 91, 1576–1588. https://doi.org/10.1002/wer.1144

Yang, L., He, L., Xue, J., Ma, Y., Shi, Y., Wu, L., Zhang, Z., 2020. UV/SO32− based advanced reduction processes of aqueous contaminants: Current status and prospects. Chem. Eng. J. https://doi.org/10.1016/j.cej.2020.125412

Yazdanbakhsh, A., Eslami, A., Moussavi, G., Rafiee, M., Sheikhmohammadi, A., 2018. Photo-assisted degradation of 2, 4, 6-trichlorophenol by an advanced reduction process based on sulfite anion radical: Degradation, dechlorination and mineralization. Chemosphere 191, 156–165. https://doi.org/10.1016/j.chemosphere.2017.10.023

Yu, H., Nie, E., Xu, J., Yan, S., Cooper, W.J., Song, W., 2013. Degradation of Diclofenac by Advanced Oxidation and Reduction Processes: Kinetic Studies, Degradation Pathways and Toxicity Assessments. Water Res. 47, 1909–1918. https://doi.org/10.1016/j.watres.2013.01.016

Yu, X., Cabooter, D., Dewil, R., 2018. Effects of process variables and kinetics on the degradation of 2,4-dichlorophenol using advanced reduction processes (ARP). J. Hazard. Mater. 357, 81–88. https://doi.org/10.1016/j.jhazmat.2018.05.049

Yu, X., Gocze, Z., Cabooter, D., Dewil, R., 2020. Efficient reduction of carbamazepine using UV-activated sulfite: Assessment of critical process parameters and elucidation of radicals involved. Chem. Eng. J. 126403. https://doi.org/10.1016/j.cej.2020.126403